NIST-GCR-96-704

FLAME BASE STRUCTURE OF SMALL-SCALE POOL FIRES

S. Venkatesh, A. Ito, K. Saito

Department of Mechanical Engineering
University of Kentucky
Lexington, KY 40506-0108

and

I.S. Wichman

Department of Mechnaical Engineering
Michigan State University
East Lansing, MI 48824-1226

December 1996

U.S. Department of Commerce
Michael Kantor, *Secretary*
Technology Administration
Mary L. Good, *Under Secretary for Technology*
National Institute of Standards and Technology
Arati Prabhakar, *Director*

This paper was presented at:
the 26th International Symposium on Combustion, 1996 and
will appear in the Proceedings.

Flame Base Structure of Small–Scale Pool Fires

S. Venkatesh, A. Ito, K. Saito*

Department of Mechanical Engineering
University of Kentucky
Lexington, KY 40506–0108

and

I.S. Wichman

Department of Mechanical Engineering
Michigan State University
East Lansing, MI 48824–1226

*Corresponding Author: K. Saito
Tel (606)257–1685, Fax (606)257–3304

Current Addresses:
(1) A. Ito, Dept. of Production Systems Engineering
Oita University, Oita, Japan
(2) S. Venkatesh, Acurex Environmental Corp.,
555 Clyde Avenue, P.O. Box 7044
Mountain View, CA 94039

Colloquium Topic:
Fundamentals of Fire Research

FLAME BASE STRUCTURE OF SMALL SCALE POOL FIRES

S. Venkatesh, A. Ito, K. Saito
University of Kentucky

and

I.S. Wichman
Michigan State University

ABSTRACT

This paper attempts to answer the question, "Why are small scale pool fires anchored?" by providing and interpreting a new set of experimental data. For momentum–controlled, high Reynolds (Re) number turbulent–jet diffusion flames, the formation of a premixing zone is suggested as the primary reason for the flame anchoring. For buoyancy–controlled pool fires, however, the existence of the premixing zone at the flame base is not clear because both Re and Fr (Froude number) are low. To improve our understanding of the flame anchoring mechanism and structure of buoyancy–controlled liquid pool fires, we employed small scale pool fires whose diameters range between 1.5 – 20 cm. Our measurements include flow visualization by a particle–track laser–sheet technique (PTLS) combined with a high speed video camera and temperature profiles by a fine thermocouple. We found from those measurements that major air entrainment occurred through the primary anchoring zone, PAZ, which consists of a small area covering approximately 1 cm high and around the circumference just above the dark zone; while air entrainment through the quenching zone (a dark zone formed between the visible flame edge and the burner port) was negligible. The structure of the PAZ was found to be premixed flame (another interpretation may be it is similar to counter–diffusion flame). This enables the pool fires to anchor at the burner port. In addition, we visualized the existence of a vortex ring at a stagnation zone in the fuel vapor phase for both propanol and hexane pool fires, in agreement with qualitative observation by other workers.

INTRODUCTION

The mechanism of air entrainment in pool fires is of current interest because of both fundamental curiosity and practical concerns related to flame extinguishment by liftoff through flame blowoff and flame instability near the burner port. In past research on buoyancy controlled pool fires, McCaffrey [1] and Cox and Chitty [2] proposed three separate zonal structures (Fig. 1): a continuous flame zone as the base of the flame, which is followed by an intermittent flame zone where active turbulent mixing takes place, and above it a plume zone where the center–line temperature begins its decrease.

Weckman and associates [3–5] performed a simultaneous measurement of velocity and temperature profiles in and around medium sized pool fires whose diameters ranged from 30 cm to 60 cm. Zhou and Gore [6] and Cetegen [7] studied flow structures of pool fires induced by buoyancy. Zhou and Gore [6] performed a series of elaborate laser–Doppler–velocimetry (LDV) and particle–image–velocimetry (PIV) measurements and obtained a velocity map around a liquid pool fire of 7.1 cm diameter. Cetegen [7] developed his unique optical measurement system and obtained a series of phase resolved velocity fields for pulsating buoyant plumes of helium–air mixtures over a 10 cm diameter nozzle. Cetegen found that the flow structure of buoyancy controlled pool fires can be simulated by helium flow moving upwardly against a quiescent air environment. The above studies [1–7] help us understand the mechanisms of flame pulsation, air entrainment, and air–fuel mixing in buoyancy controlled pool fires.

Here, we attempt to understand the mechanism of flame anchoring at the base. Our focus, therefore, differs from [1–7] and is more closely related to that of Bouhafid et al [8], who measured temperature, and species (CO, CO_2 and O_2) concentration profiles for a 15 cm diameter kerosene pool fire. Bouhafid et al. [8] observed a looped isotherm by a fine thermocouple and looped iso–CO and iso–CO_2 concentrations by a stainless steel, water cooled aerodynamic quench probe followed by an online gas chromatography analysis. They suggested that air entrainment near the base leads to fuel–air mixing by

convection giving the flame a premixed character causing pool fires to be anchored. However, their oxygen concentration profiles near the edge of the flame may not be reliable because their probe quenches chemical reactions around the probe and thereby creates a quenching area through which air can diffuse into the flame interior.

We believe that their premixing mechanism can be accurately examined using a non–intrusive flow visualization technique. Indeed, Bouhafid et al [8] made an attempt to visualize their 15 cm kerosene pool fire, but their effort was unsuccessful because of strong emissions from the kerosene flame. Therefore, we chose hexane and propanol because they are less sooty than kerosene. We conducted flow visualization, PTLS–velocity and thermocouple–temperature measurements in order to reveal detailed flow and temperature structures at PAZ.

Our objectives are:

(1) Understanding the mechanism of flame anchoring in pool fires. We investigate if and how the PAZ controls the flame anchoring. The cross–sectional area of PAZ is at most 1 cm high x 1 cm wide in radial direction consisting of the pan's brim surface, a sub–millimeter size dark (quenching) zone, a millimeter–size visible leading flame edge, and an extended (believed to be diffusion controlled) flame zone. We divided McCaffray's continuous flame zone into three subzones: the quenching zone, PAZ, and post PAZ, and studied each zone thoroughly. Figure 1 shows a schematic of the five–zone structure.

Much work has been conducted on the stability and liftoff of laminar and turbulent jet diffusion flames. The common understanding is that premixing occurs near the base and is responsible for anchoring and stabilization. The results by Takahashi et al. [9,10] on turbulent jet diffusion flames show mixing of the fuel and air through a circulation zone established at the burner rim due to strong shear stresses, leading to flame anchoring. For liquid pool fires, Bouhafid et al [8] suggested the formation of a premixed reaction zone as the mechanism of flame anchoring due to the observed strong radial component of the air velocity induced by the plume. We think that in a pool fire, the fuel

and oxidizer velocities at PAZ are much smaller, perhaps insufficient to produce shear stress induced circulation zones observed for the turbulent jet diffusion flames.

(2) Understanding of the mechanism of air entrainment at PAZ and other heights. According to Bouhafid et al [8] and this study, convective air entrainment likely occurs at PAZ in order to satisfy mass conservation because of the rapid acceleration of the buoyant gases in the flame interior. In the intermittent region, however, air entrainment occurs mainly by relatively large–scale buoyancy–induced mixing as explained by Weckman et al [3–5], Zhou and Gore [6] and Cetegen [7]. In the post–PAZ region where the flame is a pseudo laminar continuous flame, air streamlines are parallel to the visible flame surface (to be shown in Fig. 3), and air transport to the flame surface is by diffusion.

(3) Experimental confirmation of the stagnation and re–circulation zone. Based on thermocouple temperature and CO, CO_2 concentration measurement data, Bouhafid et al [8] predicted the existence of a stagnation and re–circulation zone in the fuel–vapor phase just above the liquid fuel surface. Yet there is no experimental data to directly verify their prediction; therefore, flow–visualization experiments were conducted in order to examine the proposed stagnation and re–circulation zones.

EXPERIMENTAL METHODS

Pool fire experiments were conducted at the pan's wall temperature at 20 ± 2 ^{o}C by wrapping the pan's outer wall with a 4 mm diameter copper tube and circulated water through the tube. We found the pool fire was most stable when the fuel level was 0.5 mm below the brim. Therefore, we first filled the fuel to the brim, ignited it by a small propane torch, allowed the fuel level to decrease by 0.5 mm, and applied a liquid–level controller to keep the fuel level at that position. To investigate the dependence of the flow structure on the pool diameter, stainless–steel pans of six different diameters (1.5, 3.3, 5.7, 7.8, 10 and 20 cm) and 2 cm height were designed. In this diameter range, all

the pool fires exhibited a similar flame structure shown in Fig. 1. Then, detailed measurements were conducted using the 5.7 cm diameter pan.

Flow Visualization and Velocity Measurement

We learned from the exploratory experiments that a particle–track laser–sheet technique with a high speed video camera (500 frame/s and 25 degree view angle) system (PTLS) can serve best for our measurements, because PTLS can measure profiles of both stream lines and the 2D velocity with significantly fewer particles and nearly instantaneously [11]. If the flow field is in a steady state, a 3D flow field can also be measured by rotating the cylindrical lens about the laser beam. We first checked our flow structure using this method and found that our flow profiles at PAZ are co–axial, i.e., the velocity vector possesses only the r and z components (a schematic of the experimental apparatus is shown in Fig. 1 and the flow visualization result will be presented later).

Using a 300 mW Argon–ion laser beam and a cylindrical lens, we established a thin laser sheet with an approximately 35 degree opening angle (Fig. 1). Pool fires were seeded with commercially available talc particles (its mean diameter was determined to be 3 $\pm$ 1 μm by SEM). The air stream was seeded by talc particles generated by a seeding bed located 5 cm below and away from the pan's rim (Fig. 1). To visualize the buoyancy–induced flow inside the flame sheet, a 0.5 cm diameter stainless–steel tube was welded in the co–axial location of the 5.7 cm diameter pan through which talc particles were slowly injected into the flame. Both the burning rate of fuel and the visible flame height remained unchanged with and without the seeding tube. Furthermore, we visualized the fuel–vapor flow in the flame interior near the fuel surface by seeding particles through the quenching zone and comparing these results to the above results. We did not find any difference in the results obtained by these two techniques, thus confirming that a particle injection–velocity of 7 cm/s and our low number density particles produced no significant changes in the original flow field.

Temperature Measurement

Temperature measurements were made using a 75 μm–diameter uncoated chromel–alumel thermocouple. The thermocouple was not coated because there was no difference in the temperature reading with and without the silica coating in PAZ. The effects of the conductive heat loss (or gain) through the wire and the convective heat loss (or gain) from the wire and the couple bead were estimated to cause a temperature difference in the neighborhood of $100 - 150$K, and radiation heat loss to be approximately 100 K temperature drop at the flame sheet using [12]. Because temperature fluctuations are negligible at PAZ and our pool fires produce less soot, the effect of soot deposition on the thermocouple was negligible except for a narrow (the center of the downward–pointing horn) region of the hexane flame. The best possible thermocouple shape and its insertion angle for our pool fires were experimentally determined (see Fig. 1 for a schematic).

RESULTS

Flame Appearance

A clear blue flame attaches 0.2 mm above the port, it extends 0.8 to 1 cm from the port, and it becomes invisible beyond that height. Then, a yellow luminous flame with a downward–pointing horn shape begins. There is a small range of heights where both the blue flame and the yellow flame existed. Above that zone, a luminous continuous flame followed. The double flame structure, shown in Figs. 3 and 4, was previously observed for ten different hydrocarbon–air diffusion flames under laminar over–ventilated coflow air conditions [13].

We confirmed the formation of a blue whisker flame (possibly part of a triple flame) for hexane and propanol pool fires. Then, our effort was further extended to six different fuels (methanol, acetone, pentane, octane, decane, and benzene). Because of the strong luminosity, the formation of the blue whisker flame was not clear for benzene. So,

a 1.6 cm diameter Pyrex coflow apparatus with an evaporator in the fuel line (detailed in [14]) was used and a benzene–air diffusion flame of 2 cm flame height was established. The fuel was then diluted by nitrogen. With 5 to 6 times nitrogen (by volume) dilution, the flame became less luminous and the formation of the double–flame structure became clearly identifiable.

As a result, the formation of the double–flame structure has been confirmed for 19 different fuels (hydrocarbons and alcohols) for the diameter ranges from 1 to 10 cm with and without nitrogen dilution.

Flow and Temperature Structures

For the 5.7 cm diameter propanol fire, flow structures of the air entrainment and the fuel–vapor are shown in Fig. 2, and a flow–vector diagram constructed from figures 2 results is shown in Fig. 3. Figure 4 shows a schematic of the double flame structure and tangential V_t and normal V_n components of the particle velocity V along the flame sheet as a function of vertical height from the burner port. The same measurements were conducted for the hexane pool fire, but they were not presented here because they behaved similarly.

Air entrainment through the visible flame sheet occurs just above the pan's brim and continues approximately 0.8 mm to 1 cm above the port (Fig. 3). Air entrainment at PAZ is by a smooth laminar flow suction as opposed to the intermittent zone, where it occurs by large–scale buoyancy–induced mixing. In the post–PAZ, air entrainment is only by diffusion as the velocity vectors indicate in Fig. 3. For both propanol and hexane, the ratio of air entrainment through the quenching zone to the net air entrainment at PAZ was found to be approximately 0.05.

DISCUSSION

The observed PAZ structure, where a substantial amount of air penetrates the

flame sheet by convection suggesting it can be either interpreted as premixed flame or counter–flow diffusion flame [15,16]. The authors provide experimental data on which these two interpretations based, but do not conclude which interpretation is more feasible and encourage future research on this problem.

The theoretical structure of the flame near the base or the burner rim resembles a wall–quenched triple (or tribrachial) flame, whose character has been discussed [17,18]. The general requirement is for two initially separated streams of fuel and oxidizer, which mix by molecular diffusion after flowing past a divider. Enhanced mixing may be promoted by the partial premixing of one or both reactant streams. In theory, the resultant flame structure consists of an intersection of two variable–strength premixed flames (PFs), one lean, the other rich, with a flame whose locus coincides with the stoichiometric line. The point of intersection is called the triple point (TP). Here the reaction rate is a maximum, with a value far higher than the two PF arcs. The intensely localized region of high reaction rate allows the flame structure to survive, despite the nearby hostile environment of a quenching surface. Interestingly, the gradient of the reaction rate toward the quenching surface is so high that the location of maximum reaction rate practically coincides with the quench point.

The position of the flame locus may shift depending on the overall stoichiometry. In the usual case, the flame lies on the oxidizer side in the mixture fraction coordinate Z, where $Z = 0$ in the pure oxidizer stream and $Z = 1$ in the pure fuel stream (either of which may be fictitious), and $Z = Z_f = 1/(1 + \nu)$ at the DF locus. When ν is either greater or smaller than unity, one of the two PFs may be smaller than the other, depending also on the local flow field. In the flow field examined in Fig. 3, we see that the oxidizer–side flow entering the flame is substantial, whereas the fuel–side flow is negligible. Hence, regardless of the ν–value, the fuel–side PF must be small since there is no flow against which it may propagate. The oxidizer–side PF, however, propagates against the vigorous entrained air flow. Therefore, the oxidizer–side PF is by far the

more vigorous. This argument may explain the double–flame structure that is observed, although blockage of the small fuel–side flame may hamper visualization.

Concerning stoichiometry, we observed that the six fuels examined here are methanol ($\nu = 1.5$, $Z_f = 0.4$), propanol ($\nu = 4.5$, $Z_f = 0.182$), acetone ($\nu = 4.5$, $Z_f = 0.182$), pentane ($\nu = 8$, $Z_f = 0.111$), hexane ($\nu = 9.5$, $Z_f = 0.0952$), and octane ($\nu = 12.5$, $Z_f = 0.0741$), all of which have $\nu > 1$ and $Z_f < 0.5$. Color photographs of the flame in the air entrainment zone were taken, their images were projected on a screen, and their relative positions were measured [19]. As ν increases and Z_f decreases, the entrainment–zone diameter d increased as the flame moved toward the oxidizer side (smaller Z_f): $d_{oct} > d_{hex} > d_{prop} > d_{acet} > d_{meth}$. Hence, the observed flame structure is consistent with the nature of the flow field and the change of flame position is consistent with the stoichiometry. Note that, however, acetone (molecular weight, 58.05) and 1–propanol (molecular weight, 60.09) possess different air–entrainment–zone diameters. This suggests that beside the effect of stoichiometry, ν, often parameters like pyrolysis rates, preferential diffusion, flame temperature and burning rates also influence the location of the flame sheet.

Why is the Double Flame Instead of the Triple Flame Observed?

We observed the double flame instead of the triple flame. This fact needs to be discussed here. A rather detailed discussion of triple (or tribrachial) flame propagation into an opposing flow of partially premixed gases has been given by Chung and Lee [20], who argue that the tribrachial flame propagates with a speed very close to the stoichiometric flame speed. This hypothesis has some theoretical support from the calculations of Dold [21] and others for the case of free or isenthalpic flames far from cold surfaces. Near cold surfaces, where the flame may suffer substantial enthalpy losses, this hypothesis breaks down entirely. In fact, flames may attach without any opposed flow at all. That is, pure diffusion flames can attach to cold and chemically frozen regions simply

through the creation of upstream mixing regions (formulas for the quenching distance were given [17]).

Regarding the above question, it is important to pay attention to the fact that the velocity of air flow in the air side is one order of magnitude higher than the velocity of fuel vapor in the fuel side and the visible flame sheet is located in the air stream side. Although a relatively strong air current is crossing the flame sheet and convecting into the flame interior (Figs. 3 and 4), the fuel vapor will eventually diffuse to the flame. Thus, the oxidizer side PF is expected to be much larger than the fuel side PF. As demonstrated in Figs. 2 and 3, the flame at PAZ possesses characteristics of the counter diffusion flame, yet the existence of the cold wall quenches the flame and likely to distort the normal (or free boundary) triple flame into the double flame.

Temperature Structure

Radial temperature profiles at different heights are shown in Figs. 5a and 5b; both fuels exhibit a steep temperature gradient on the air side. The flame sheet temperature (peak temperature) is greater for n–hexane than 1–propanol near the base. The measured temperature near the base appears to be consistent with recent theoretical results [22], which showed an extinction temperature, 1230 ^{o}C based on three step chemical reactions rather than a one–step overall reaction. In the yellow (sooty) region, z = 5 and 10 mm in Figs. 5a and 5b, the flame sheet temperature of propanol is greater than hexane. This may be because of the larger radiation losses and uncertainties in the thermocouple temperature measurements in the hexane flame where the thermocouple was coated (only at the limited location, Z = 10 mm in Fig. 5a) with soot particles causing a rapid decrease in its output reading.

Flame Anchoring Mechanism

Takahashi and Schmoll [10] have shown that for the turbulent jet diffusion flames,

the mechanism of anchoring depends on the formation of shear–stress related circulation zones. Due to shearing between the fuel jet, whose flow speed may be much higher than the flame propagation speed, and the oxidizer, a stagnant circulation zone is developed where mixing occurs and the flame is allowed to anchor. They proved that when a burner with a tapered rim was used, the flame was not able to anchor or stabilize. However, our data show that in a pool fire, the shear stresses at the rim are lower by two orders of magnitude compared to the jet diffusion flame [10] demonstrating insignificance of shear–stress induced mixing. This suggests that the mechanism of anchoring of a flame in a buoyancy dominated pool fire and a momentum–force dominated jet diffusion flame are different. Nevertheless, both anchoring mechanisms require the generation and sustained presence of a mixing zone, where fuel and oxidizer can intermix. The mechanisms by which these two flames produce these zones are quite distinct.

We believe that in PAZ the structure of the flame sheet is similar to a triple flame although only the double structure was observed here. Because of finite–rate chemistry influences, the flame sheet has a finite thickness. Because the DF is bounded on either side by two PFs, we may introduce the concept of the flame propagation speed. We focus on the outer (oxygen–rich) PF. The direction of the flame propagation vector is opposite to the tangential component of the entrainment vector, V_t. If V_t is greater than the flame propagation speed near the base, the flame won't be able to anchor or stabilize, as shown by Takahashi and Schmoll [10] by using a tapered burner. We confirmed from our PTLS measurements (Figs. 3 and 4) that V_t in the convective–air entrainment zone was lower than the stoichiometric flame speeds (propanol, 0.34 m/s and hexane 0.42 m/s).

To experimentally prove this, we designed a 15 cm diameter Pyrex–chimney and attached it to the 5.7 cm–diameter pool fire burner in a coaxial location. The aim of this experiment is to prove that when the air velocity exceeds V_t, the pool fire will lift off from the base. This burner system was designed based on the concept of our coflow hydrocarbon–air diffusion–flame burner [13]. The air was supplied from a compressed air

cylinder through an air filter; its volumetric flow–rate was controlled and measured by a rotameter. Normal propanol and hexane were used as fuel, external air was seeded by the talc particles, and the r–z velocity components of air at and near PAZ was measured by PTLS. Our experiments demonstrated that the pool fires can anchor at the burner rim provided the tangential component of the air velocity V_t is less than approximately 0.3 m/s (because of the page limitation, the data is not presented here and see ref. [19]). With the slight increase of V_t, the flame suddenly become unstable causing a sudden liftoff of the flame, and sometime causing reattachment of the flame to the rim. With further increase of V_t, a steady lift–off of the flame occurred. The flame can be anchored at the rim or it can be lifted–off to the height where the main flame begins. The leading edge of the flame was quite unstable at PAZ and could not anchor at any PAZ region [19].

SUMMARY AND CONCLUSIONS

In reference to the three specific objectives addressed in the **Introduction**, the conclusions obtained from this study are summarized here.

(1) Based on our experimental measurements on pool fires in diameter of 1.5 – 20 cm of propanol and hexane, and finite–rate chemistry concepts, the entire flame sheet of a pool fire is established to have a triple flame structure. The structure of the flame at the base was established from PTLS data and through a comparison of the location of the flame sheet in the convective–air entrainment zone for fuels with different stoichiometric fuel–air requirements.

(2a) Air entrainment through the quenching zone was found to be a small fraction of the net air entrainment near the base for the pool fires. Our data show that the ratio of the total mass of air entrained into the flame interior through PAZ to the total mass of air entrained through the quenching zone was 0.05.

(2b) The fluid–dynamic structure of the anchoring mechanism of a

buoyancy–dominated small scale pool fire and a momentum–dominated jet diffusion flame is different. In a jet diffusion flame, the Reynolds shear stress near the rim of the burner induces a stagnant re–circulation zone where the fuel and the oxidizer are mixed and the flame anchors. To the contrary, in a pool fire the shear stresses at the rim are two orders of magnitude lower and turbulent mixing does not occur [23]. Finite–rate chemistry establishes the presence of a molecular–diffusion mixing zone. Therefore, the flame anchors at the base.

(3) For both propanol and hexane pool fires with their diameter range between 1.6 cm and 10 cm, the formation of the stagnation re–circulation zone predicted by Bouhafid et al [8] was experimentally confirmed.

ACKNOWLEDGEMENTS

We would like to thank F.A. Williams, A.S. Gordon and T. Hirano for their valuable comments. This study was supported in part by the National Institute of Standards and Technology under grant #60NANB4D1674, in part by NASA–Kentucky EPSCoR program and in part by the Center for Manufacturing Systems at the University of Kentucky.

REFERENCES

1. McCaffrey, B.J., **Combustion and Flame,** 52: 149–167 (1983).

2. Cox, G. and Chitty, R., **Combustion and Flame**, 39: 191–209 (1980).

3. Weckman, E.J., **Ph.D. Thesis,** University of Waterloo, Ontario, Canada, 1987.

4. Weckman, E.J. and Sobiesiak, A, **Twenty–second International Symposium on Combustion,** The Combustion Institute, 1988, pp. 1299–1310.

5. Wechman, E.J. and McEwen, C.S, **ASME/JSME Joint Thermal Engineering Conference,** Vol. 5, 1991.

6. Zhou, X.C., and Gore, J., **Combust. Flame,** 100: 52–60 (1995).

7. Cetegen, B., "Phase–resolved Velocity Field Measurements in Pulsating Buoyant Plumes of Helium–Air Mixtures," presented at **the Annual NIST Fire Research Conference,** Gaithersburg, MD., October 20, 1994.

8. Bouhafid, A.,Vantelon, J.P., Joulain, P. and Fernandez–Pello, A.C., **Twenty–second International Symposium on Combustion,** The Combustion Institute, 1988, pp. 1291–1298.

9. Takahashi, F., Mizomoto, M., Ikai, S., and Futaki, N., Twentieth International Symposium on Combustion, The Combustion Institute, 1985, pp. 295–302.

10. Takahashi, F. and Schmoll, W.G., **Twenty–third International Symposium on Combustion,** The Combustion Institute, 1990, pp. 677–683.

11. Hirano, T., Sato, K. and Tazawa, K., **Combust. Flame,** 26: 191–200 (1976).

12. Kaskan, W.E., Tenth International Symposium on Combustion, The Combustion Institute, 1960, pp. 134–143.

13. Saito, K., Williams, F.A., and Gordon, A.S., **Combust. Sci. Tech.**, 51: 291–312 (1987).

14. Sidebotham, G., Saito, K. and Glassman, I., **Combust. Sci. Tech.**, 85: 283–296 (1991).

15. Williams, F.A. **Combustion Theory,** Benjaming/Cummings, 1985.

16. Tsuji, H., **Prog. Energy and Combust. Sci.**, 8: 93–119 (1982).

17. Wichman, I.S., **Combust. Sci. Tech.**, 64: 295–313 (1989).

18. Wichman, I.S., "Basic Features of Triple Flames in Combustion Theory," to appear **8th ISTP,** July, 1995.

19. Venkatesh, S., Ito, A., and Saito, K., ME Report, Dept. of Mechanical Engineering, University of Kentucky, Lexington, KY 40506, 1994.

20. Chung, S.H., and Lee, B.J., **Combust. Flame,** 86: 62–72 (1991).

21. Dold, J.W., **Combust. Flame,** 76: 71–72 (1989).

22. Card, J.M. and Williams, F.A., **Combust. Sci. Tech.**, 84: 91–119 (1992).

Figure Captions

Figure 1 A schematic of the three zone structure for small pool fires and a schematic of particle–track laser–sheet (PTLS) flow visualization apparatus.

Figure 2 PTLS photographs for the flow fields for a 5.7 cm diameter hexane pool fire: (a) at and around PAZ, and (b) inside the flame sheet and near the fuel surface.

Figure 3 Profiles of 2D velocity fields for a 5.7 cm diameter hexane pool fire constructed from the figure 2 results.

Figure 4 Tangential velocity component, V_t and normal velocity component, V_n measured by PTLS along the flame sheet and at different vertical height from the burner port, Z.

Figure 5 Radial distribution of the temperature near the base for five different heights: (a) hexane, and (b) 1–propanol. (The thermocouple bead was coated with soot only at Z = 10 mm of the hexane flame; all other points for both propanol and hexane flames are free from the soot deposit).

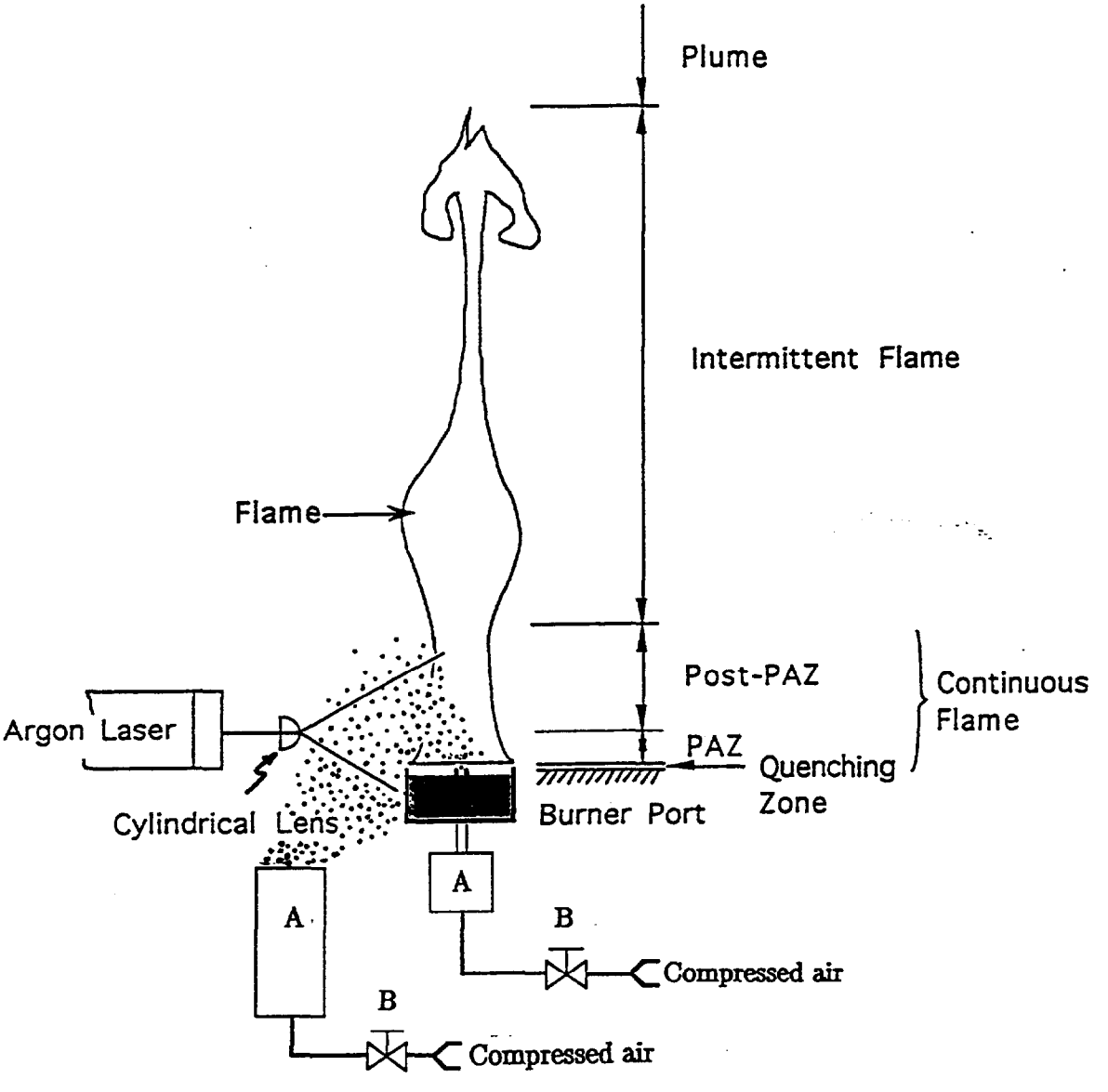

A: Particle feeder

B: Control valve

Venkatesh et at Fig. 1

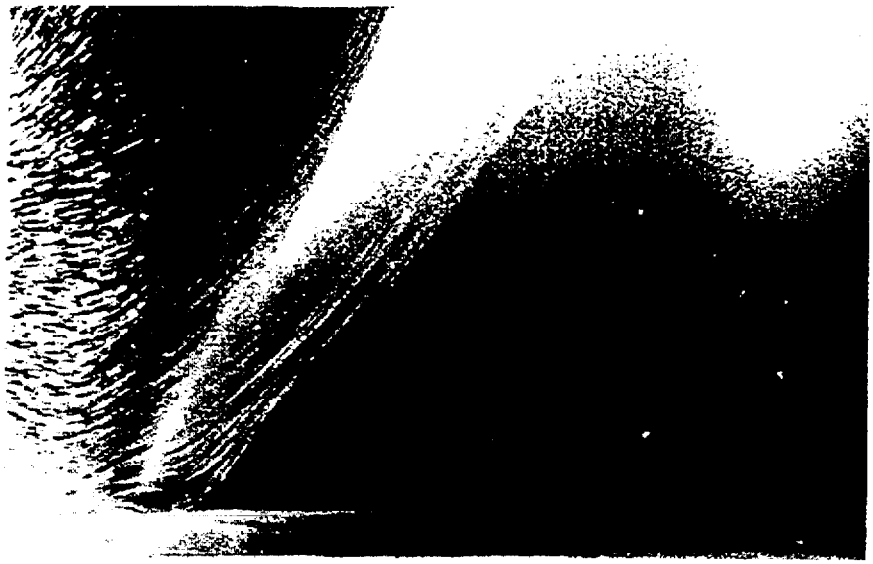

(a)

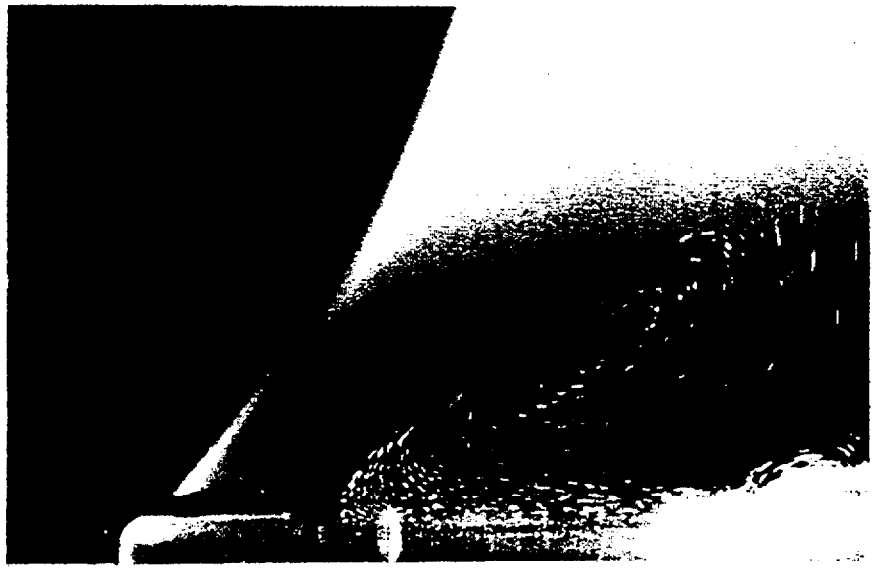

(b)

Venkatesh et al Fig. 2

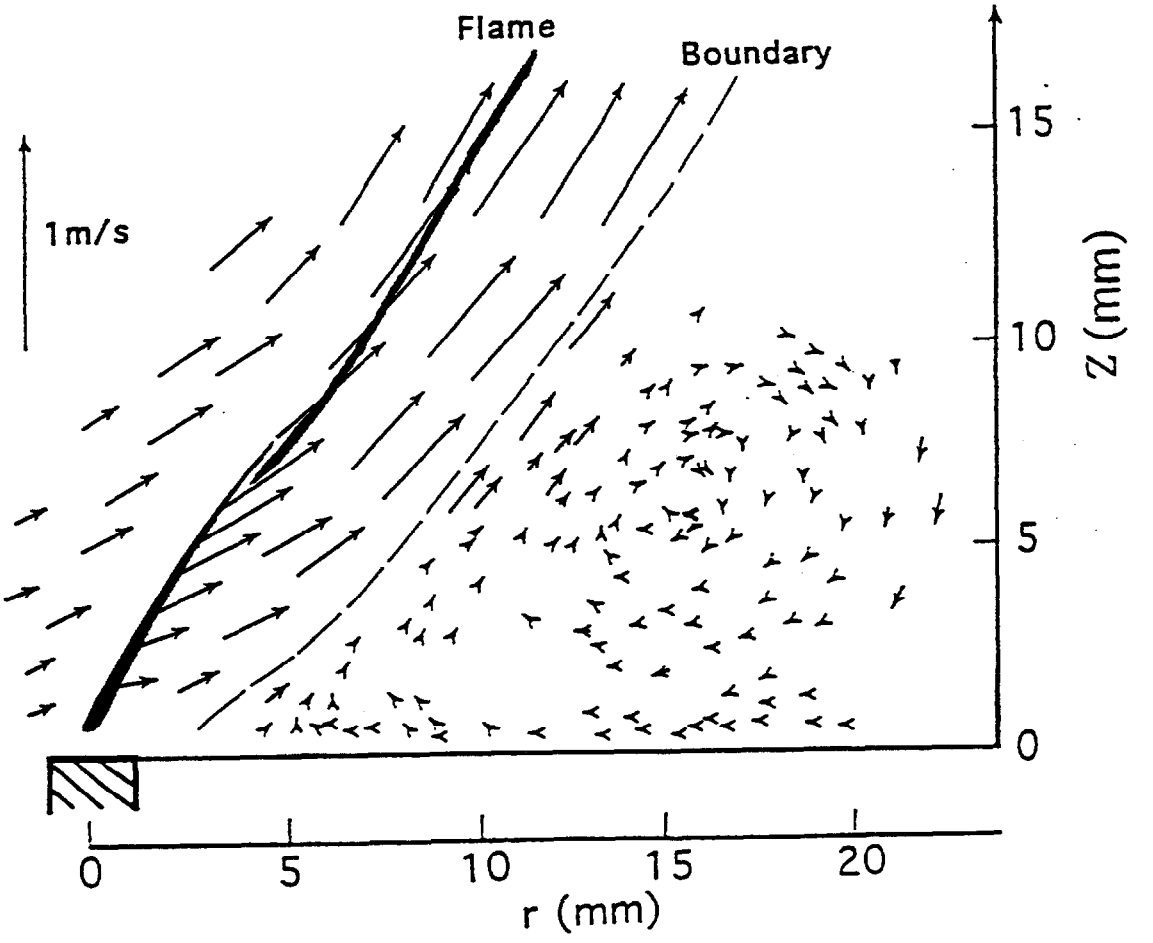

Venkatesh et al Fig. 3

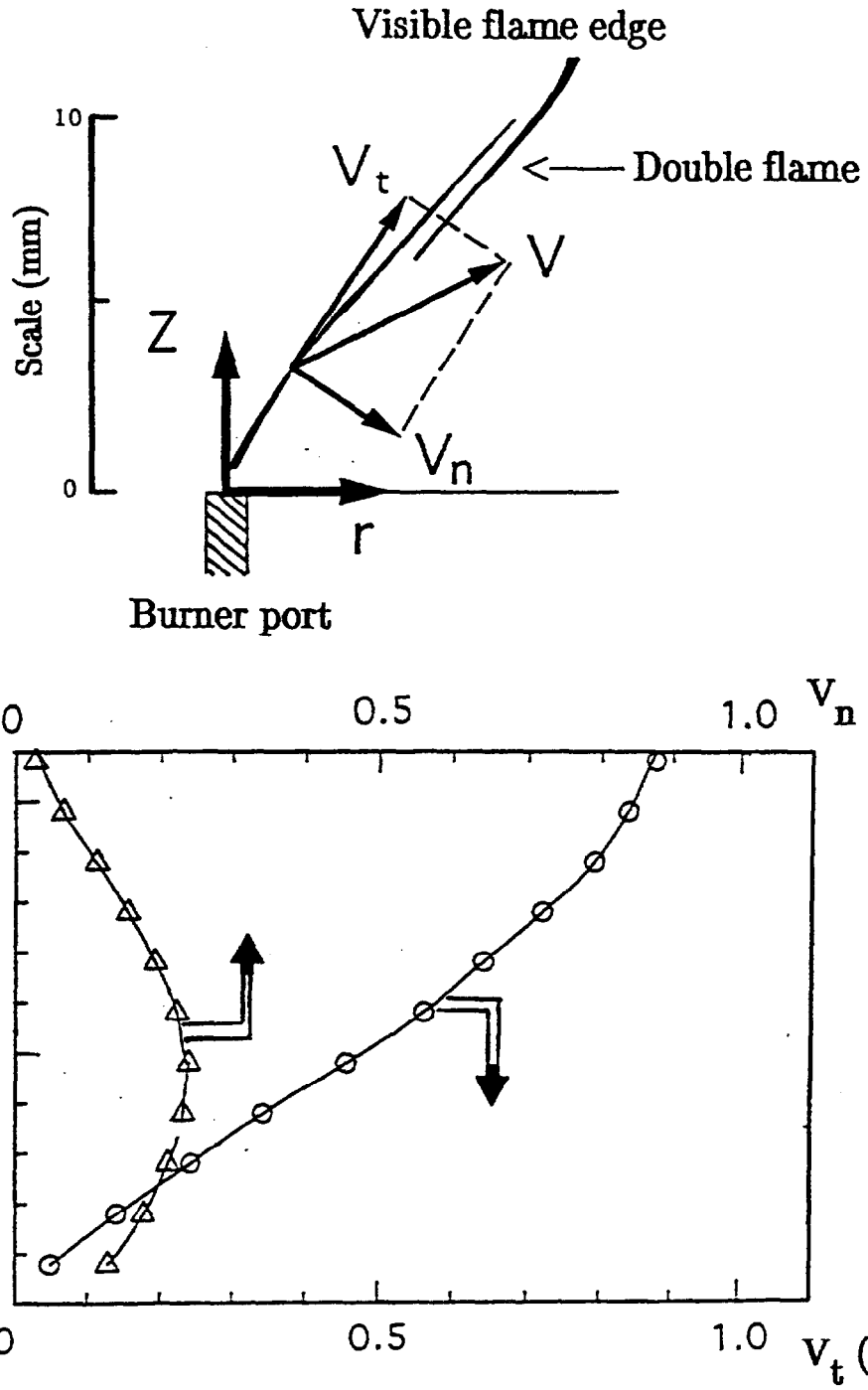

Venkatesh et al Fig. 4

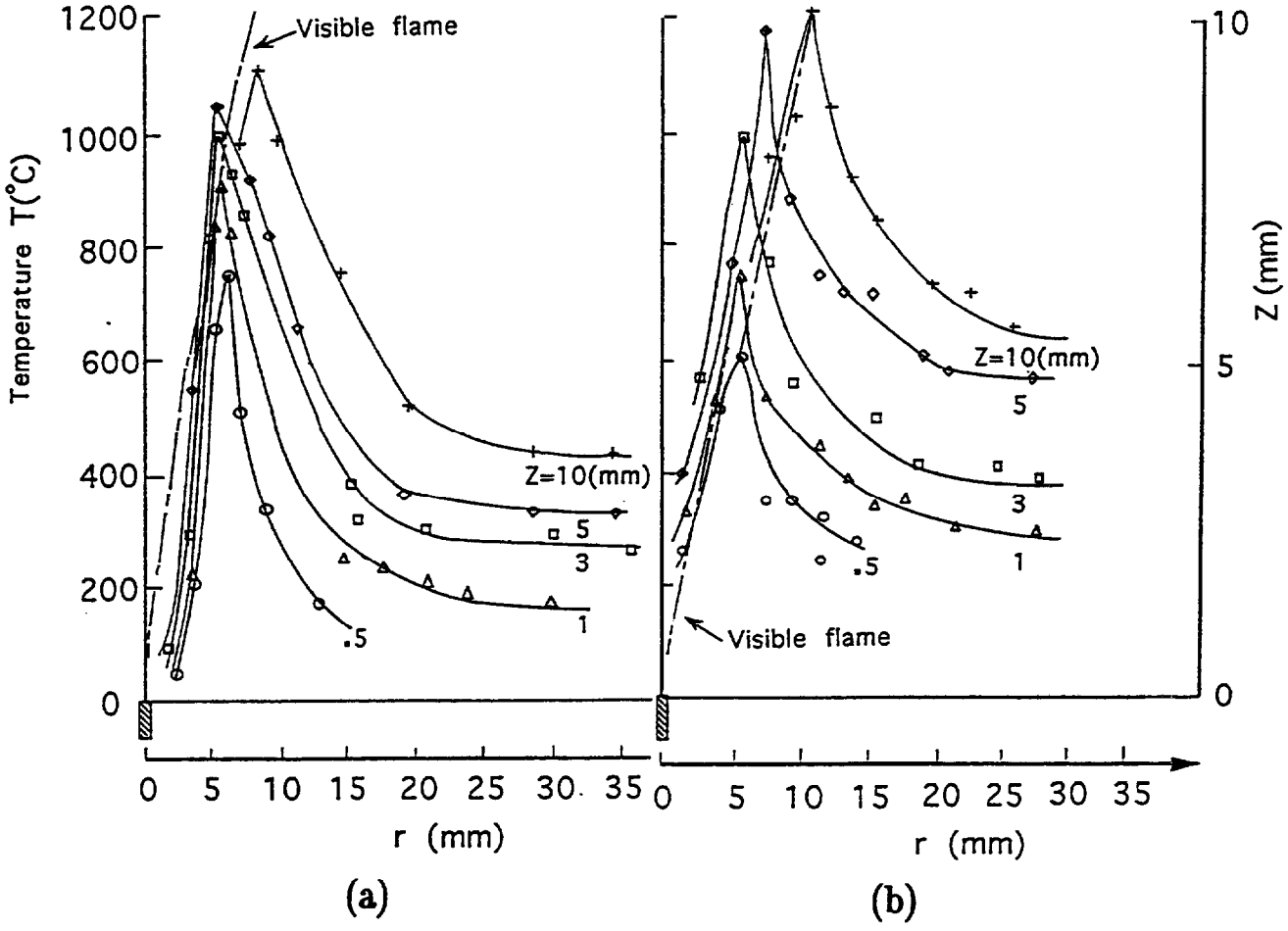

Venkatesh et al Fig. 5